Sensor Fusion for Shape Reconstruction Using Electromagnetic Tracking Sensors and Multi-Core Optical Fiber

Ha, Xuan Thao; Wu, Di; Ourak, Mouloud; Borghesan, Gianni; Menciassi, Arianna; Poorten, Emmanuel Vander

DOI
10.1109/LRA.2023.3280456

Publication date
2023

Document Version
Final published version

Published in
IEEE Robotics and Automation Letters

Sensor Fusion for Shape Reconstruction Using Electromagnetic Tracking Sensors and Multi-Core Optical Fiber

Xuan Thao Ha, Di Wu, *Graduate Student Member, IEEE*, Mouloud Ourak, Gianni Borghesan, Arianna Menciassi, *Fellow, IEEE*, and Emmanuel Vander Poorten, *Member, IEEE*

***Abstract*—Optical fiber-based shape sensing is gaining popularity in cardiac catheterization lately. Typically, these procedures are taking place under the guidance of fluoroscopy. However, fluoroscopy has several disadvantages. Thanks to fiber optic shape sensing and Electromagnetic Tracking (EMT), the 3D catheter shape can now be tracked in real-time without the need for fluoroscopy. Traditional optical fiber and EMT-based shape tracking methods have the drawback of the highest shape sensing error at the tip. The information offered by the EMT sensors is used mainly to localize the estimated shape in a fixed coordinate frame. In this letter, a novel approach for tracking the catheter is introduced to address the aforementioned problem. The catheter shape is directly reconstructed in the EMT coordinate frame by approximating the catheter shape by a number of Bézier curves while taking into account the curvatures measured by the optical fiber. Both 2D and 3D shape sensing experiments are conducted. The results of the 3D experiment show that the proposed method reduces the mean shape tracking error by approximately 38% (from 12.1 mm to 5.4 mm for a sensed length of 540 mm long) compared to the traditional method where the same number of sensors are used.**

***Index Terms*—Surgical robotics: steerable catheters/needles, sensor fusion, shape sensing, optical fiber, electromagnetic tracking.**

I. Introduction

IN THE last 10 years, advances in minimally invasive surgery (MIS) have influenced practically every specialty in medicine. Patients benefit from MIS by having less pain, fewer surgical and post-operative significant problems, a shorter hospital stay, and faster recoveries. Flexible devices (*e.g.* catheters and guidewires) are normally used to reach the operation site through narrow and tortuous vessels in these MIS procedures. Catheter navigation is normally performed under the guidance of fluoroscopy. However, fluoroscopic images only provide 2D visualization of medical devices and anatomy. This leads to poor awareness of where the catheter is in the vessel and consequently complicates devising the optimal steering actions to execute the navigation task. Moreover, radiation emitted from fluoroscopy and contrast agents utilized in the process are harmful to patients as well.

To overcome these problems, different sensor modalities have been proposed in the literature to track the 3D shape of the catheters. A method to reconstruct the 3D shape of a flexible instrument using biplane fluoroscopy was proposed by Wagner et al. in [1]. Radiation is still a problem here since biplane fluoroscopy results in higher radiation doses compared to monoplane fluoroscopy [2]. EMT sensors have been embedded in flexible devices to track their shapes during the procedure [3], [4], [5]. In these approaches, the shape of the flexible device is approximated by multiple Bézier curves. However, these approaches require a relatively high number of EMT sensors to be integrated to achieve sufficient accuracy. Especially catheters which are typically long and flexible, many EMT sensors are needed which makes them complex and fragile. Besides the large number of EMT sensors, another disadvantage of the EMT-based shape sensing method is that the measurement accuracy is affected by the presence of ferromagnetic materials. To solve this problem, Tran et al. proposed fusing the shape estimated by the EMT-based method with fluoroscopic images [6]. Alternatively, the method proposed in [7] fuses EMT-based shape with a predictive model of the catheter. This fusing approach is radiation-free. However, a concrete model of the catheter is difficult to achieve. Moreover, the extensibility of this approach is a problem since extra effort is needed to model the flexible devices accurately.

Fiber optic-based approaches are becoming increasingly common in catheter shape sensing lately [8], [9], [10], [11], [12] due to the fiber's biocompatibility, compact size, lightweight, and flexibility. This shape sensing approach relies on strains measured along the fiber's length. Strain sensing technologies based on fiber optics can be categorized into quasi-distributed sensing (Fiber Bragg Grating) and distributed sensing (Rayleigh scattering-based and Brillouin scattering-based method). Fiber Bragg Gratings (FBG) are the most widely used technique these days thanks to their high frequency data acquisition

Manuscript received 27 March 2023; accepted 4 May 2023. Date of publication 29 May 2023; date of current version 5 June 2023. This letter was recommended for publication by Associate Editor S. Zuo and Editor P. Valdastri upon evaluation of the reviewers' comments. This work was supported in part by ARTERY Project through European Union's Horizon 2020 Research and Innovation Programme under Grant 101017140 and in part by CURE a KU Leuven Internal Project under Grant 3E210658. *(Corresponding author: Xuan Thao Ha.)*

Xuan Thao Ha is with the Department of Mechanical Engineering, KU Leuven, 3000 Leuven, Belgium, and also with The BioRobotics Institute, Scuola Superiore Sant-Anna, 56025 Pontedera, Italy (e-mail: xuanthao.ha@kuleuven.be).

Di Wu is with the Department of Mechanical Engineering, KU Leuven, 3000 Leuven, Belgium, and also with the Faculty of 3mE, TU Delft, 2628 CD Delft, The Netherlands (e-mail: di.wu@kuleuven.be).

Mouloud Ourak and Emmanuel Vander Poorten are with the Department of Mechanical Engineering, KU Leuven, 3000 Leuven, Belgium (e-mail: mouloud.ourak@kuleuven.be; Emmanuel.VanderPoorten@kuleuven.be).

Gianni Borghesan is with the Department of Mechanical Engineering, KU Leuven, 3000 Leuven, Belgium, and also with Flanders Make, 3920 Lommel, Belgium (e-mail: gianni.borghesan@kuleuven.be).

Arianna Menciassi is with The BioRobotics Institute, Scuola Superiore Sant-Anna, 56025 Pontedera, Italy (e-mail: arianna@sssup.it).

Digital Object Identifier 10.1109/LRA.2023.3280456

ability [13]. In this work, FBG technology is used to demonstrate our proposed method. Regardless of the strain sensing technology, the remaining process for estimating the 3D shape of the fiber remains the same. Discrete curvatures along the length of the catheter can be measured by incorporating a multi-core FBG fiber into the catheter's central channel. Using the observed discrete curvatures, the method proposed by Moore and Rogge [14] can then be used to reconstruct the 3D shape of the catheter. Al-Ahmad et al. proposed methods to further improve the FBG-based catheter shape sensing accuracy in [11] showing promising experimental results. One of the disadvantages of using a multi-core fiber in a straight configuration for 3D shape sensing is that it cannot distinguish the strain induced by bending from the strain induced by twisting. Due to this reason, a small amount of twisting can greatly affect the accuracy of the overall shape reconstruction. Fusion approaches to compensate for the effect of twisting the fiber have been presented in the literature [12], [15]. These approaches still have the problem of radiation from fluoroscopy. An alternative method that addresses the twist problem is shape sensing using helical multi-core fibers [16], [17]. However, due to the high price of the twisted multi-core fiber, the multi-core fibers in a straight configuration are still favorable. Another problem of traditional FBG-based shape sensing methods (in both straight and helical configurations) is that the measured curvatures are integrated along the fiber length to reconstruct the 3D shape. In this integrating process, the error in curvature measurement accumulates. The largest shape sensing error will therefore typically appear at the fiber tip. Moreover, fiber optic-based shape sensing only offers information about the 3D catheter shape expressed in the grating's local coordinate frame. This is a coordinate frame that is coincidentally fixed with the most proximal grating. For making use of that information, it is important to have the reconstructed shape expressed in an external preferably static reference. To localize the 3D shape reconstructed in a fixed coordinate frame, additional EMT sensors have been proposed to be integrated into the catheter [10], [12]. In this letter, we propose a new catheter tracking approach based on a combination of EMT sensors and a multi-core FBG fiber. The newly proposed approach allows incorporating the information from the EMT sensors in the 3D shape reconstruction process itself, which helps to solve the aforementioned problems. Unlike the traditional approach, the 3D catheter shape will be approximated here by multiple Bézier curves. Compared to the state-of-the-art EMT sensors-based shape sensing method [3], [4], [5], our Bezier curve fitting process not only uses the pose information from the EMT sensors but also uses the curvature measured by the FBG fiber. This approach aids in reducing the number of integrated EMT sensors. The problem of error build-up by integrating the errors over the measurement length in the classic FBG-based shape sensing method is now resolved since the tip point and other points along the catheter length are now constrained by information provided by the EMT sensors. An advantage of the proposed method is that the EMT sensors information is now, not only to localize the reconstructed shape in a global coordinate frame but also helps improve the estimated shape. A further advantage of the proposed fusion approach is that without explicit modeling of the dynamic twist, the effect of dynamic twist acting on the straight configuration multi-core fiber is also compensated. It is worth noting that although the multi-core FBG fiber is used here to demonstrate the proposed approach, the approach can be easily transferred to other fiber optic-based shape sensing techniques (in both straight and helical configurations). A set of 2D and 3D experiments are done to demonstrate the value of the proposed approach. The traditional EMT and FBG-based and EMT-based catheter tracking methods are also implemented and serve as a baseline against which the newly proposed approach is compared to. The experimental results show that the new estimation method outperforms the traditional approach in both 2D and 3D experiments.

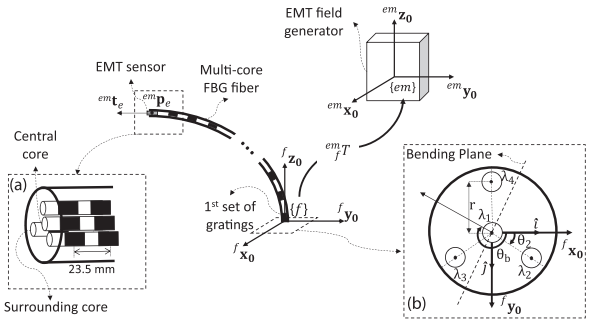

Fig. 1. Relation between EMT coordinate frame {em} and the FBG local coordinate frame {f} that is coincidentally fixed with the 1st set of gratings is shown in this figure. A side and a cross-section view of the multi-core FBG fiber can be seen in (a) and (b), respectively. The angle of the bending plane and the angle of the 2nd core with respect to the x-axis are denoted as θ_b and θ_2 in (b), respectively.

The rest of the letter is organized as follows: Section II details the newly proposed catheter tracking method. Experiments to validate the proposed method are described in Section III. Finally, Section IV concludes the work and sketches some future directions.

II. Method

FBG-based shape sensing methods rely on measured discrete curvatures and bending plane angles along the length of a fiber. These curvatures are obtained by employing an interrogator to monitor the change in the reflected wavelength of each grating. A method to calculate the curvature and the angle of the bending plane from the measuring wavelength shift is described in Section II-A. In the traditional approach, the 3D shape of the catheter in the FBG local coordinate frame {f} is then reconstructed using the method proposed in [11]. Afterward, the 3D shape is localized in the fixed EMT coordinate frame {em} as explained in [12] by using additional information from the EMT sensors. The relation between {f} and {em} coordinate frames is described in Fig. 1. The traditional 3D shape reconstruction and localization process are briefly summarized in Section II-B. In Section II-C, the newly proposed catheter tracking approach is detailed.

A. Curvature and Angle of Bending Plane

Fig. 1(a) and (b) depict the construction of a multi-core FBG fiber. A multi-core FBG fiber commonly has four cores. The first core is located in the center and aligns with the neutral axis of the fiber. There are three surrounding cores at a distance of r from the central core. These cores are spaced 120° rotated around the central core. Each core features the same number of gratings distributed along its length. Each grating is a Bragg reflector that reflects a particular wavelength of the incoming

light while transmitting all others. The central wavelength of the reflected light of each grating is named the Bragg wavelength λ_B. The reflected wavelengths are measured by an interrogator connected to the proximal end of the multi-core FBG fiber. The wavelength of each grating varies depending on the change of the surrounding temperature ΔT and the applied mechanical strain ϵ. The measured wavelength shift is given by:

$$\frac{\lambda_B - \lambda_{B_0}}{\lambda_{B_0}} = \frac{\Delta\lambda}{\lambda_{B_0}} = S_\epsilon \epsilon + S_T \Delta T, \tag{1}$$

where S_ϵ and S_T are the strain and temperature sensitivity coefficients of the fiber, respectively. λ_{B_0} is the unstrained Bragg wavelength of the grating. The gratings in the central core are only sensitive to axial strain and temperature variations. When the axial strain is negligible, as is commonly the case with catheters, the wavelength changes due to temperature variations can then be computed from this central core. The bending strain applied on the outer cores $\epsilon_{Bend_{i\in\{2,3,4\}}}$ can subsequently be determined as follows:

$$\epsilon_{Bend_{i\in\{2,3,4\}}} = \frac{\Delta\lambda_i}{\lambda_{B_{0i}} S_\epsilon} - \frac{\Delta\lambda_1}{\lambda_{B_{01}} S_\epsilon}. \tag{2}$$

As such the multi-core fiber allows measuring three bend induced strains per cross-section where a set of gratings is present. These strains can then be used to calculate the curvature κ_{FBG} and the angle of the bending plane $\theta_{b_{FBG}}$ at each measurement cross-section. The relation between the bend induced strain, the curvature, and the angle of the bending plane is given by:

$$\epsilon_{Bend_{i\in\{2,3,4\}}} = -\kappa_{FBG} r \sin\left(\theta_{b_{FBG}} - \frac{3\pi}{2} - \theta_i\right), \tag{3}$$

where r is the distance from the outer cores to the central core; θ_i is the angle of the ith outer core and $\theta_{b_{FBG}}$ the angle of the bending plane corresponding to the x-axis of the fiber (as shown in Fig. 1(b). Moore and Rogge proposed a closed-form solution for (3) in [14] given by:

$$\begin{aligned} \boldsymbol{\kappa}_{app} &= \sum_{i=2}^{4} \frac{\epsilon_{Bend_i}}{r} \cos\theta_i \hat{i} - \sum_{i=2}^{4} \frac{\epsilon_{Bend_i}}{r} \sin\theta_i \hat{j}, \\ \kappa_{FBG} &= \frac{2|\boldsymbol{\kappa}_{app}|}{3}, \\ \theta_{b_{FBG}} &= \angle \boldsymbol{\kappa}_{app}, \end{aligned} \tag{4}$$

where $\hat{i}$ and $\hat{j}$ are the unit vectors along the x- and y-axes of the fiber's cross-section, respectively, as depicted in Fig. 1(b).

B. Traditional EMT and FBG-Based Catheter Tracking Approach

A traditional FBG-based catheter tracking approach includes two main steps. Firstly, the catheter shape is estimated in the local coordinate frame that is defined here, without loss of generality, to coincide with the most proximal grating of the fiber. The 3D reconstructed shape of the catheter is then localized in the global EMT coordinate frame by exploiting the information provided by the attached EMT sensors. The 3D catheter shape estimation process based on the discrete curvatures and the angles of the bending plane is briefly discussed in Section II-B1. Section II-B2 describes the catheter shape localization process.

1) Traditional FBG-Based Catheter Shape Estimation: The set of discrete curvatures and the angles of the bending plane are first interpolated to improve the estimated shape and maintain a quasi-continuous curvature profile along the catheter's arc length. Assuming that the entire arc length of the catheter is discretized into u points, the sets of the interpolated curvatures and angles of the bending plane are denoted as $\boldsymbol{\kappa}_{FBG_{int}}$ and $\theta_{b_{FBG_{int}}}$, respectively. A continuous and differentiable space curve can be used to represent the shape of the catheter. This space curve is defined by curvature $\kappa(s)$ and torsion $\tau(s)$ profiles with the arc length variable s that changes from $s = 1$ at the first set of grating to $s = u$ at the last set of grating. The torsion $\tau(s)$ is the rate of change of the angle of the bending plane θ_b along the fiber length. The interpolated curvature and torsion profiles define how the tangent **t**, normal **n**, and binormal **b** unit vectors (TNB frame) evolve along the arc length. The differential Frenet-Serret formula [18] can be used to solve for the evolution of the moving TNB frame. The position **c**(s) of each point along the catheter shape can then be calculated by integrating the tangent unit vectors as follows:

$${}^f\mathbf{c}(s) = {}^f\mathbf{c}(1) + \int_1^s \mathbf{t}(v)dv, \tag{5}$$

where ${}^f\mathbf{c}(1)$ is the position of the catheter's base.

2) Catheter Shape Localization in EMT Coordinate Frame: To localize the reconstructed 3D shape of the catheter in a fixed EMT coordinate frame {em}, a spatial calibration step needs to be done in advance. Since the relative pose of {f} versus {em} may vary due to manufacturing. The following calibration procedure can be conducted to retrieve this information. First, the catheter is fixed at the level of the most proximal EMT sensor. It is then bent in planar in two configurations symmetric with respect to the straight configuration. The distance between the first and second configuration of each corresponding point at a given arc length along the 3D reconstructed shape is computed. The travel distance of each point along the length of the reconstructed shape is then compared to the travel distance of each distal EMT sensor. This allows for devising the corresponding arc length where each EMT sensor is located. After that, the distance between the most proximal sensor to the distal EMT sensors is calculated. This can be done when the catheter is in a straight configuration. From the distance between the proximal and the distal EMT sensors in the straight configuration and the correspondence between the distal EMT sensors to the 3D shape reconstructed shape, the correspondence of the proximal sensor can then be estimated. Details on the spatial calibration procedure can be found in [19].

Assuming that m EMT sensors are attached to the catheter and the pose measured by each EMT sensor corresponds to the pose of a point along the arc length of the FBG-based 3D reconstructed shape ${}^f\mathbf{c}(s_{EMT_i})$ where $i = \{1, \ldots, m\}$, the 3D shape of the catheter can then be localized in the EMT coordinate frame. The correspondence arc length of the ith EMT sensor s_{EMT_i} is estimated by the above-mentioned spatial calibration step. Each EMT sensor provides its location ${}^{em}\mathbf{p}_{e_i}$ and its unit tangent vector ${}^{em}\mathbf{t}_{e_i}$ in the EMT coordinate frame. A set of poses (including position and tangent vector) provided by the EMT sensors in {em} and their correspondences in {f} can be used to obtain the transformation matrix ${}^{em}_{f}\mathbf{T}$ *e.g.* by using a point-to-point registration method [20]. This transformation matrix then transforms the reconstructed shape from the local

frame {f} to the fixed EMT coordinate frame {em} [12]. The catheter shape in the EMT coordinate frame can be obtained by ${}^{em}\mathbf{c}(s) = {}^{em}_{f}\mathbf{T}^{f}\mathbf{c}(s)$.

C. Proposed EMT and FBG-Based Catheter Tracking Approach

The traditional method presented in the previous section requires first reconstructing the shape. The EMT sensors are only used to find the transformation matrix to map the reconstructed shape to the EMT frame. In the newly proposed approach, the catheter shape is directly reconstructed in the EMT coordinate frame in a single step. The proposed approach uses the information from the EMT sensors not only to localize the catheter shape but also to improve the shape estimation. The catheter shape is approximated by multiple Bézier curves. A Bézier curve of degree n is specified by $n+1$ control points and is defined as:

$$\mathbf{b}(t) = \sum_{i=0}^{n} \binom{n}{i} (1-t)^{n-i} t^{i} \mathbf{p}_{c_i}, \tag{6}$$

where $\binom{n}{i}$ are the binomial coefficients and $t \in [0;1]$; $\mathbf{p}_{c_i}$ are the control points. The Bézier curve starts at $\mathbf{p}_{c_0}$ and ends at $\mathbf{p}_{c_n}$. The two control points $\mathbf{p}_{c_1}$ and $\mathbf{p}_{c_{n-1}}$ lie along tangent vectors at the starting and the end point.

Assuming that m EMT sensors spaced at regular intervals are included along the length of the catheter, the catheter shape between two consecutive jth and $j+1$th EMT sensors can then be approximated by a Bézier curve. The first control point $\mathbf{p}_{c_0}$ and the last control point $\mathbf{p}_{c_n}$ of the Bézier curve between two subsequent EMT sensors can be defined by ${}^{em}\mathbf{p}_{e_j}$ and ${}^{em}\mathbf{p}_{e_{j+1}}$, respectively. An optimization problem can then be formulated to find the remaining control points $(\mathbf{p}_{c_1}, \ldots, \mathbf{p}_{c_{n-1}})$ by minimizing the cost function

$$\text{argmin}_{\mathbf{x}=\mathbf{p}_{c_1},\ldots,\mathbf{p}_{c_{n-1}}} \alpha E_{length} + \beta E_{\kappa} \tag{7}$$

where E_{length} is the error in the length of the estimated Bézier curve. Theoretically, the length of the estimated Bézier curve would be equal to the arc length between two consecutive EMT sensors jth and $j+1$th (denoted as $l_{Straight}$). The arc length $l_{Straight}$ can be measured by putting the catheter in a straight configuration. The length error E_{length} is calculated as:

$$E_{length} = (l_{Straight} - l_{Estimate})^2 \tag{8}$$

The arc length of the estimated Bézier curve can be derived analytically [21] or via numerical integration. The error in curvature E_{κ} is the difference between the curvature along the length of the estimated Bézier curve κ_B and the curvatures obtained from the FBG sensors over the corresponding section $\kappa_{FBG_{int}}(s = s_{EMT_j}, \ldots, s_{EMT_{j+1}})$. Given that the estimated Bézier curve is discretized into u_b points ($u_b = s_{EMT_{j+1}} - s_{EMT_j}$), the error in curvature E_{κ} between the jth and $j+1$th EMT sensor can be computed as:

$$E_{\kappa} = \sum_{s=s_{EMT_j}}^{s_{EMT_{j+1}}} (\kappa_{FBG_{int}}(s) - \kappa_B(t))^2 \tag{9}$$

where $t = \frac{s - s_{EMT_j}}{u_b}$. The curvature $\kappa_B(t)$ of a parameterized curve can be calculated as:

$$\kappa_B(t) = \frac{||\mathbf{b}'(t) \times \mathbf{b}''(t)||}{||\mathbf{b}'(t)||^3} \tag{10}$$

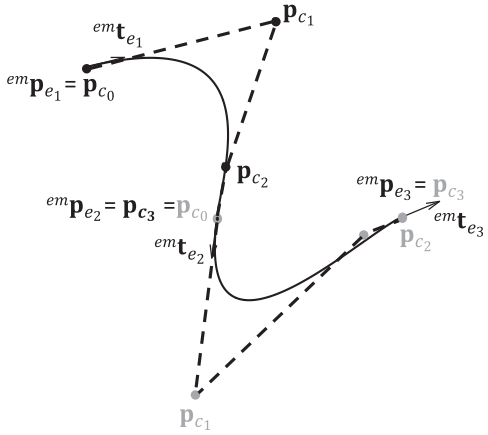

Fig. 2. An example of fitting a catheter with three integrated EMT sensors by 3rd order Bézier curves. Here, two Bézier curves are utilized to approximate the catheter shape. The first Bézier curve starts at ${}^{em}\mathbf{p}_{e_1}$ and ends at ${}^{em}\mathbf{p}_{e_2}$. The second Bézier curve starts at ${}^{em}\mathbf{p}_{e_2}$ and ends at ${}^{em}\mathbf{p}_{e_3}$. The control points of the first and second Bézier curve are colored in black and gray, respectively.

The scaling factors α and β regulate the relative weight between $E_{l_{length}}$ and E_{κ}. The optimization problem described in (7) strives to identify the control points of a Bézier curve that aligns in curvature with the curvatures measured by the optical fiber and has the same length as the arc distance between two consecutive EMT sensors.

In case the shape between two consecutive EMT sensors is approximated by a Bézier curve of degree n, $n-1$ control points need to be solved. Each control point is defined by three scalar values. Thus $3 \times (n-1)$ variables are searched for in the optimization problems. Since $\mathbf{p}_{c_1}$ and $\mathbf{p}_{c_{n-1}}$ are the two control points that lie along tangent vectors at the starting and end point, the set of optimization variables for a Bézier curve of degree n is now reduced to $3 \times (n-1) - 4$ elements $\mathbf{x} = \{l_{start}, l_{end}, \mathbf{p}_{c_2}, \ldots, \mathbf{p}_{c_{n-2}}\}$. Then, $\mathbf{p}_{c_1}$ and $\mathbf{p}_{c_{n-1}}$ can then be calculated as:

$$\begin{aligned} \mathbf{p}_{c_1} &= \mathbf{p}_{c_0} + l_{start}\ {}^{em}\mathbf{t}_{e_j} \\ \mathbf{p}_{c_{n-1}} &= \mathbf{p}_{c_n} - l_{end}\ {}^{em}\mathbf{t}_{e_{j+1}} \end{aligned} \tag{11}$$

An example of fitting the catheter shape by 3rd order Bézier curves is shown in Fig. 2.

The choice of the degree of the Bézier curve depends on the complexity of the shape that the catheter can take on between two consecutive EMT sensors. The higher degree Bézier curve can represent more complex shapes. However, as the Bézier curve's degree increases, there are more control points that the optimization problem solver must find. For this reason, this work investigates only 3rd and 4th order Bézier curves.

Different solvers can be used to tackle this optimization problem such as the trust-region reflective [22] or Levenberg-Marquardt [23]. Most of the solvers accept an initial guess for the value of each optimization parameter. The quality of the initial guess impacts the ability to converge to a global or local minimum and the speed of the convergence. To have a good initial guess for the missing control points, it is proposed here to use the traditional approach (presented in Section II-B) as a first guess to estimate the catheter shape in the EMT coordinate frame. The shape between two consecutive EMT sensors provided by the traditional approach is approximated by a Bézier

curve. The control points of the approximated Bézier curve can then be used as the initial guess for the optimization problem solver. To approximate a segment by a Bézier curve, the matrix form of the Bézier curve, based on the control points, can be used. The control points of 3rd and 4th order Bézier curves can be approximated by

$$\begin{bmatrix} \mathbf{p}_{c_0} \\ \mathbf{p}_{c_1} \\ \mathbf{p}_{c_2} \\ \mathbf{p}_{c_3} \end{bmatrix} = \left(\begin{bmatrix} \mathbf{t^3} & \mathbf{t^2} & \mathbf{t} & \mathbf{1} \end{bmatrix} \begin{bmatrix} -1 & 3 & -3 & 1 \\ 3 & -6 & 3 & 0 \\ -3 & 3 & 0 & 0 \\ 1 & 0 & 0 & 0 \end{bmatrix} \right)^{+} {}^{em}\mathbf{c} \tag{12}$$

and

$$\begin{bmatrix} \mathbf{p}_{c_0} \\ \mathbf{p}_{c_1} \\ \mathbf{p}_{c_2} \\ \mathbf{p}_{c_3} \\ \mathbf{p}_{c_4} \end{bmatrix} = \left(\begin{bmatrix} \mathbf{t^4} \mathbf{t^3} \mathbf{t^2} \mathbf{t1} \end{bmatrix} \begin{bmatrix} 1 & -4 & 6 & -4 & 1 \\ -4 & 12 & -12 & 4 & 0 \\ 6 & -12 & 6 & 0 & 0 \\ -4 & 4 & 0 & 0 & 0 \\ 1 & 0 & 0 & 0 & 0 \end{bmatrix} \right)^{+} {}^{em}\mathbf{c}, \tag{13}$$

respectively where $\mathbf{t}_{u_b \times 1} = \begin{bmatrix} \frac{1-1}{u_b-1} & \frac{2-1}{u_b-1} & \dots & \frac{u_b-1}{u_b-1} \end{bmatrix}^T$. The matrix ${}^{em}\mathbf{c}$ is a $u_b \times 3$ matrix that contains the catheter shape in {em} (corresponding to the arc length $s = s_{EMT_j}$ to $s_{EMT_{j+1}}$) estimated by the traditional method.

III. Experimental Validation

Both 2D and 3D experiments are performed to verify the proposed method. In the 2D experiment, optical markers are used with a camera to generate ground truth shapes. An advantage of the 2D experiment is that it allows for examining the accuracy of our proposed catheter tracking method in different cases (using different numbers of integrated simulated EMT sensors) with minimal effort in preparing different catheters at this stage. This is only feasible in the 2D experiment since each optical marker offers a location as well as a tangent vector. However, in practical situations, the catheter is often bent into 3D shapes. Due to this reason, 3D experiments are also performed. Unlike the 2D experiment, ground truths in the 3D experiments are acquired by fiducials attached along the fiber length tracked by a 3D real-time optical tracking system.

A. 2D Experiment

To verify the proposed catheter tracking approach and compare it with the traditional FBG-based catheter tracking method, a dilator (Abbott, USA) with an embedded multi-core FBG fiber (FBGS, Geel, Belgium) in the central channel has been prepared. The schematic of the sensorized dilator is shown in Fig. 3(a). The fiber includes four cores. Each core features 24 gratings with a spacing of 23.5 mm between each set of gratings. With this configuration, the fiber is able to sense a 540 mm long shape. There are 15 optical markers attached along the dilator's length with a spacing of 20 mm. In the 2D experiment, the dilator is bent into different shapes on the 2D plane. An overhead monocular camera (Prosilica, Allied Vision Technology, Germany) is positioned above the setup, facing downwards, to capture the dilator's shape. The recognized shapes in the images are used as the ground truth. The dilator is supported on a plexiglass plate to ensure that the bending is in a plane parallel to the image plane.

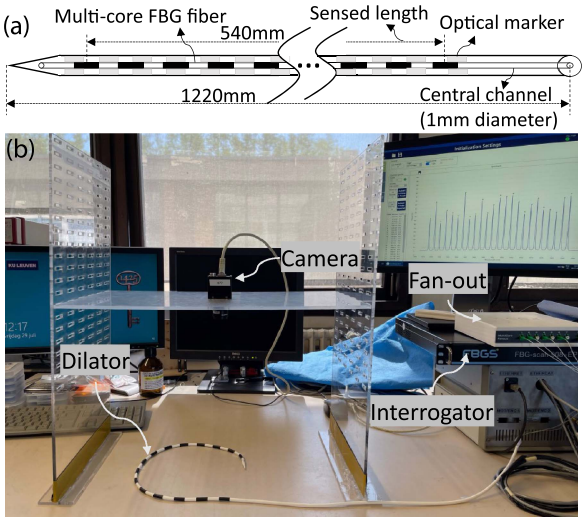

Fig. 3. Schematic in (a) shows the dimension of the sensorized dilator and how the multi-core FBG fiber is integrated. (b) The experimental setup for the 2D experiment includes the sensorized dilator, a monocular camera to capture the 2D shape of the dilator, a fan-out (to guide light from a four-core fiber into four separate channels), and an interrogator.

An interrogator (FBG-scan 908 EP) from FBGS is used to record the wavelength shifts during the experiments. The experimental setup for 2D experiments can be seen in Fig. 3(b).

Since the dilator only experiences in-plane bending, it is straightforward to use optical markers to simulate the EMT sensors. In the first case, three optical markers (the 1st, 8th and 15th marker) are used to simulate EMT sensors and to reconstruct the shape of the dilator while in the second case, four optical markers (the 1st, 5th, 10th and 15th marker) are used. In both cases, the shapes between two consecutive optical markers are approximated by 3rd and 4th order Bézier curves. Simple color segmentation is used to recognize the optical markers in the image frame. The position of the optical markers is defined as the centroid of the contour of each marker. The ground truth shape is obtained by fitting a B-spline curve to the set of positions of all optical markers. The tangent vector of each marker is calculated by taking the first derivative of the fitted B-spline curve. A known-size checkerboard is used to find the scale factor that allows transforming the recognized ground truth shape from pixel to mm scale. A sequence of the ground truth generation process is visualized in Fig. 4.

Using the measured wavelength shifts and the marker poses, the traditional and the proposed catheter tracking approaches are applied to estimate the shape of the dilator in the image coordinate frame. The EMT-based shape sensing method presented in previous work [5] is also implemented to estimate the catheter shape. The performances of the three methods are compared via shape estimation error for each dilator's configuration. The shape estimation error is calculated by the mean and max distance between each point along the length of the estimated shape to the closest point from the ground truth shape. The closest points between two sets of points can be found by using the MATLAB (The MathWorks, Inc., Massachusetts, United States) function *dsearchn*.

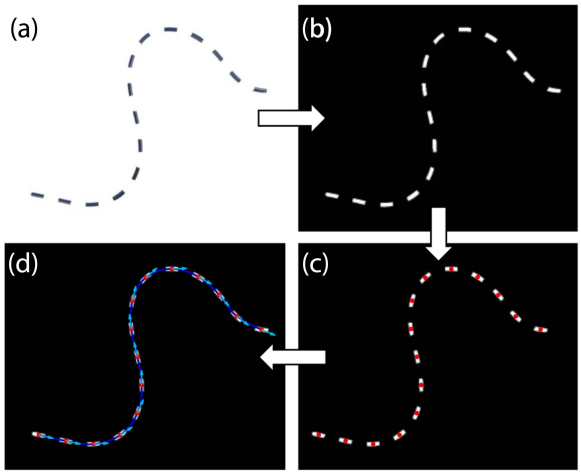

Fig. 4. An image captured by the camera is visualized in (a); (b) color segmentation is applied on the input image to segment the contour of the optical markers; (c) the centroids of the contours (red markers) of the optical markers are defined as the optical marker positions in the image coordinate frame; (d) the set of positions of all optical markers are approximated by a B-spline curve (blue). This B-spline curve is used as the ground truth shape. The tangent vectors (cyan) are calculated by taking the first derivative of the approximated B-spline curve.

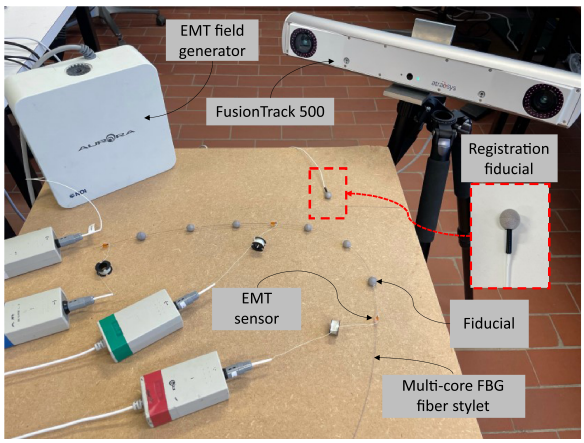

Fig. 5. The 3D experiment setup contains the EMT field generation, fusionTrack 500 system, and a multi-core FBG fiber stylet. Three EMT sensors and six spherical fiducials are attached along the length of the stylet. The registration fiducial is used to register between the EMT coordinate frame and the fusionTrack coordinate frame.

B. 3D Experiment

In the 3D experiment, a multi-core FBG stylet from FBGS has been used. The stylet includes a multi-core FBG fiber inserted into a Nitinol tube. The fiber contains four cores each core includes 39 gratings with a spacing of 14 mm. This multi-core fiber allows measuring a shape of 532 mm long. Three EMT sensors are attached to the stylet at approximately the 1st, 20th, and 39th grating by means of 3D printed fixtures. The stylet has six spherical fiducials spaced evenly over its length. The 3D positions of these spherical fiducials can be tracked by a real-time optical pose-tracking system - fusionTrack 500 (Atracsys, Puidoux, Switzerland). The 3D experiment setup is described in Fig. 5.

In this experiment, the stylet is bent into different configurations. The 3D shape of the stylet is reconstructed in the EMT coordinate frame by both the traditional and the proposed method using the information provided by the FBG fiber and the three EMT sensors. The 3D positions of the fiducials recognized by the fusionTrack system (accuracy of 0.09 mm) are used as ground truth. The EMT coordinate frame and the fusionTrack coordinate frame need to be registered in advance. To register these two coordinate systems, a registration fiducial has been prepared. This registration fiducial features an EMT sensor inserted into the central channel of the spherical fiducial. The registration fiducial is manually moved in the tracking space of the EMT system and the fusionTrack system. The registration fiducial's 3D positions in the two coordinate frames are utilized to find a transformation matrix to map the position in the fusionTrack coordinate frame to the EMT coordinate frame. The transformation matrix is found by using a point-to-point registration method [20]. Three catheter tracking approaches including a pure EMT-based approach (presented in [5]), the traditional approach (EMT+FBG), and the newly proposed approach (EMT+FBG) are used to estimate the stylet shape. The shape estimation error is calculated by the distance between each spherical fiducial's position to its closest point from the reconstructed shape.

C. Results and Discussion

The experimental results of the 2D experiment are shown in Fig. 6. In the 1st case, three pose sensors are used while in the 2nd case, four pose sensors are used. The shapes estimated by both the traditional and the proposed method using four pose sensors are shown in Fig. 6(a)–(f). For each case, the shape reconstruction error of the traditional method, the proposed method using 3rd order Bézier curve and 4th order Bézier curve, and the EMT-based method are presented in green, orange, cyan, and magenta in Fig. 6(g) and (h), respectively. Experimental results show that the proposed method improves the tracking accuracy by approximately 50% and 70% (compared to the traditional method) in the case where three and four pose sensors are used, respectively. The largest difference in the shape tracking error between using the 3rd and 4th order Bézier curve can be seen in the 5th shape (Fig. 6(e)) where three pose sensors are used. This is due to the fact that an nth order Bézier curve can only change direction along an axis at most $n-1$ times. Hence, a 3rd order Bézier curve cannot properly represent the shape of a segment with more than two direction changes. The average shape tracking error when three and four pose sensors are used together with FBG are 2.4 mm and 0.9 mm, respectively for a 540 mm sensed length. It can be seen that the purely EMT-based catheter tracking approach does not provide consistent accuracy compared to the EMT and FBG-based approaches. The EMT-based shape sensing accuracy varies depending on the complexity of the catheter shape. This conclusion is in line with our previous work [5].

The 2D experimental results have shown that the 4th order Bézier curve outperforms the 3rd order Bézier curve in reconstructing a complex dilator shape. For this reason, only 4th order Bézier curve is used to estimate the 3D shape of the stylet in the 3D experiment. In the 3D experiment, the FBG stylet is bent into four configurations. The shape estimation results using the traditional method, the newly proposed method with a 4th order Bézier curve and the EMT-based method are shown in blue,

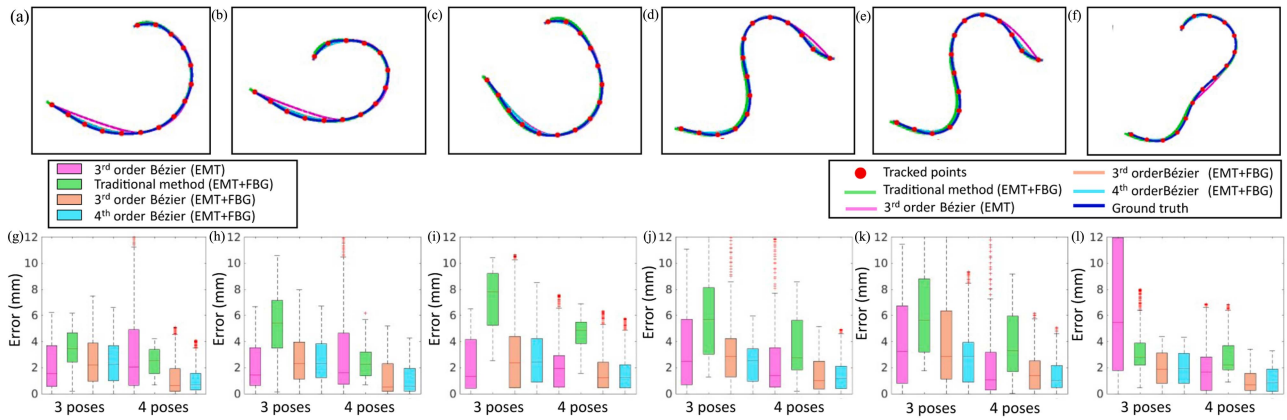

Fig. 6. Reconstructed shapes in the image coordinate frame of the 2D experiments using four pose sensors can be seen in (a)–(f). The shapes reconstructed by the traditional method (EMT+FBG) is shown in green while the shape reconstructed by the proposed method using 3rd and 4th order Bézier curves (EMT+FBG) are shown in orange and cyan, respectively. The shapes estimated by the EMT-based method are shown in magenta. The blue curves show the ground truth shape. The red circles are the tracked optical markers. Fig. (g) and (h) show the error (in mm) of the traditional method (EMT+FBG), the proposed method (EMT+FBG), and the method in which only EMT sensors are used in two cases - using three pose sensors (1st case) and using four pose sensors (2nd case).

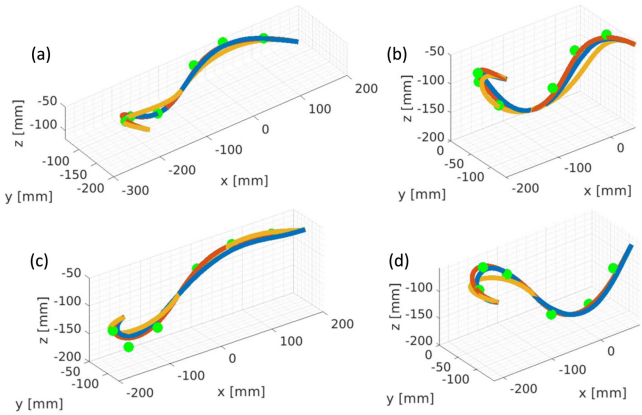

Fig. 7. Reconstructed shapes together with the fusionTrack fiducials of the 3D experiment are expressed in the EMT coordinate frame. The shapes reconstructed by the traditional method (EMT+FBG) are shown in blue while the shapes reconstructed by the proposed method using 4th order Bézier curves are shown in orange (EMT+FBG). The yellow curves show the shape estimation results by using only EMT sensors. The fusionTrack fiducials (green) are transformed to the EMT coordinate frame using the transformation matrix obtained from the pre-registration step.

TABLE I
THE MEAN AND MAX ERROR OF THE RECONSTRUCTED SHAPES IN THE 3D EXPERIMENT USING THE TRADITIONAL METHOD(EMT+FBG), THE NEWLY PROPOSED METHOD WITH 4th ORDER BÉZIER CURVE(EMT+FBG) AND THE METHOD IN WHICH ONLY EMT SENSORS ARE USED

	EMT + FBG				EMT	
	Traditional method		Proposed method (4th order Bezier curve)			
	Mean	Max	Mean	Max	Mean	Max
a	8.0 ± 4.0	12.2	3.8 ± 2.9	7.6	11.9 ± 5.6	17.2
b	11.1 ± 3.6	16.6	5.9 ± 2.8	11.3	16.2 ± 7.0	26.0
c	$8.4 + 2.9$	12.5	6.9 ± 3.7	14.1	10.2 ± 7.7	24.1
d	7.0 ± 2.2	10.2	5.1 ± 2.1	7.5	10.1 ± 6.7	22.6

orange, and yellow in Fig. 7, respectively. The mean and max shape reconstruction errors of the three methods are reported in Table I. The 3D experimental results show that by using the proposed method, the shape tracking accuracy increases by 38% compared to the traditional method. Our proposed method outperforms the EMT-based catheter tracking method by 55%. Currently, the proposed algorithm is implemented in MATLAB and can run at 10 Hz and 4 Hz in the case of the 3rd and 4th order Bézier curve, respectively. Solving the optimization problem for the control points is the most time-consuming task in the proposed shape tracking algorithm. The processing time, however, can be reduced by using parallel computing [24] while solving the optimization problems. It is worth mentioning that one does not expect too fast shape variations in this sort of application. According to [25], the most frequently used framerate of fluoroscopy for traditional minimally invasive procedures is 7.5 Hz. The current implementation of our proposed method in case of 3rd order Bézier curve is already equally fast (but does not cause radiation). One can note that the shape tracking error of the traditional FBG-based shape sensing method reported here is significantly larger than other results reported in the art [10], [11], [12]. This is due to the fact that in these works, the reconstructed shape is typically aligned with the ground truth by means of a point cloud registration (Iterative Closest Point algorithm [26] or point-to-point registration method) before the shape sensing error is calculated. These point cloud registration methods actively reduce the error between the estimated shape and the ground truth. Unlike these previous works, the shape tracking frame (EMT coordinate frame) and the ground truth frame (fusionTrack frame) are pre-registered and we do not resort to ICP. One of the disadvantages of the traditional FBG-based shape sensing method is that the largest shape sensing error normally appears at the tip of the fiber. This problem is caused by the fact that the shape is reconstructed by integrating the measured curvatures along the fiber length. The here proposed method does not suffer from this problem. The fiber shape is now approximated as a set of Bézier curves where the tip and the base pose of each segment are defined by EMT sensors. The proposed algorithm is general and can be applied to catheters with different numbers of integrated EMT

sensors. The 2D experimental results show that by increasing the number of the integrated EMT sensors, the shape tracking accuracy tends to improve as shown in the 2D experiment (20% improvement when using four pose sensors compared to using three pose sensors).

IV. Conclusion

In this letter, a new approach to track the 3D shape of the catheter using information provided by a multi-core optical fiber and a certain number of EMT sensors is proposed. The new approach reconstructs the catheter shape by approximating the catheter by a set of Bézier curves. Unlike the traditional FBG-based shape tracking method, where the FBG-based reconstructed shape is localized in a global frame using a point-to-point registration method, the proposed catheter shape tracking method directly reconstructs the catheter shape in the EMT coordinate frame. By approximating the catheter shape by multiple Bézier curves, the problem of the largest shape sensing error appearing at the tip of the catheter can be avoided. Experiments in 2D and 3D have been done to verify the proposed method. The EMT-based method and the traditional EMT and FBG-based shape tracking method are also implemented to serve as a baseline. The results of the 2D experiment show that the proposed approach outperforms the traditional approach. The performance increases by approximately 50% and 70% in the case of three pose sensors and four pose sensors are used, respectively. The same pattern can be seen in the 3D experiment where the new method improves the shape tracking accuracy by approximately 38% compared to the traditional method. The combination of multi-core optical fiber and EMT sensors allows real-time tracking of the catheter during the procedure with high accuracy. The proposed approach may eliminate the need for fluoroscopy, therefore lowering harmful radiation exposure to both patients and clinicians. Animal tests will be done in the future to evaluate the performance of the proposed shape sensing algorithm.

References

[1] M. Wagner, S. Schafer, C. Strother, and C. Mistretta, "4D interventional device reconstruction from biplane fluoroscopy," *Med. Phys.*, vol. 43, no. 3, pp. 1324–1334, 2016.

[2] V. Sadick, W. Reed, L. Collins, N. Sadick, R. Heard, and J. Robinson, "Impact of biplane versus single-plane imaging on radiation dose, contrast load and procedural time in coronary angioplasty," *Brit. J. Radiol.*, vol. 83, no. 989, pp. 379–394, 2010.

[3] S. Song, Z. Li, H. Yu, and H. Ren, "Electromagnetic positioning for tip tracking and shape sensing of flexible robots," *IEEE Sensors J.*, vol. 15, no. 8, pp. 4565–4575, Aug. 2015.

[4] S. Song, Z. Li, M. Q. H. Meng, H. Yu, and H. Ren, "Real-time shape estimation for wire-driven flexible robots with multiple bending sections based on quadratic bézier curves," *IEEE Sensors J.*, vol. 15, no. 11, pp. 6326–6334, Nov. 2015.

[5] X. T. Ha, I. Tamadon, M. Ourak, G. Borghesan, A. Menciassi, and E. Vander Poorten, "Comparative study on electromagnetic tracking and fiber Bragg grating-based catheter shape sensing," in *Proc. IEEE Sensors*, 2022, pp. 1–4.

[6] P. T. Tran et al., "3D catheter shape reconstruction using electromagnetic and image sensors," *J. Med. Robot. Res.*, vol. 2, no. 03, 2017, Art. no. 1740009.

[7] A. Dore, G. Smoljkic, E. Vander Poorten, M. Sette, J. Vander Sloten, and G.-Z. Yang, "Catheter navigation based on probabilistic fusion of electromagnetic tracking and physically-based simulation," in *Proc. IEEE/RSJ Int. Conf. Intell. Robots Syst.*, 2012, pp. 3806–3811.

[8] C. Shi, S. Giannarou, S.-L. Lee, and G.-Z. Yang, "Simultaneous catheter and environment modeling for trans-catheter aortic valve implantation," in *Proc. IEEE/RSJ Int. Conf. Intell. Robots Syst.*, 2014, pp. 2024–2029.

[9] F. Khan, A. Denasi, D. Barrera, J. Madrigal, S. Sales, and S. Misra, "Multi-core optical fibers with Bragg gratings as shape sensor for flexible medical instruments," *IEEE Sensors J.*, vol. 19, no. 14, pp. 5878–5884, Jul. 2019.

[10] S. Jäckle et al., "Three-dimensional guidance including shape sensing of a stentgraft system for endovascular aneurysm repair," *Int. J. Comput. Assist. Radiol. Surg.*, vol. 15, no. 6, pp. 1033–1042, 2020.

[11] O. Al-Ahmad, M. Ourak, J. V. Roosbroeck, J. Vlekken, and E. V. Poorten, "Improved FBG-based shape sensing methods for vascular catheterization treatment," *IEEE Robot. Automat. Lett.*, vol. 5, no. 3, pp. 4687–4694, Jul. 2020.

[12] X. T. Ha et al., "Robust catheter tracking by fusing electromagnetic tracking, fiber Bragg grating and sparse fluoroscopic images," *IEEE Sensors J.*, vol. 21, no. 20, pp. 23422–23434, Oct. 2021.

[13] I. Floris, J. M. Adam, P. A. Calderón, and S. Sales, "Fiber optic shape sensors: A comprehensive review," *Opt. Lasers Eng.*, vol. 139, 2021, Art. no. 106508.

[14] J. P. Moore and M. D. Rogge, "Shape sensing using multi-core fiber optic cable and parametric curve solutions," *Opt. Exp.*, vol. 20, no. 3, pp. 2967–2973, 2012.

[15] M. Ourak et al., "Fusion of biplane fluoroscopy with fiber Bragg grating for 3D catheter shape reconstruction," *IEEE Robot. Automat. Lett.*, vol. 6, no. 4, pp. 6505–6512, Oct. 2021.

[16] F. Khan, D. Barrera, S. Sales, and S. Misra, "Curvature, twist and pose measurements using fiber bragg gratings in multi-core fiber: A comparative study between helical and straight core fibers," *Sensors Actuators A: Phys.*, vol. 317, 2021, Art. no. 112442.

[17] I. Floris, J. Madrigal, S. Sales, P. A. Calderón, and J. M. Adam, "Twisting measurement and compensation of optical shape sensor based on spun multicore fiber," *Mech. Syst. Signal Process.*, vol. 140, 2020, Art. no. 106700.

[18] T. F. Banchoff and S. T. Lovett, *Differential Geometry of Curves and Surfaces*. Boca Raton, FL, USA: AK Peters/CRC, 2010.

[19] X. T. Ha et al., "Shape sensing of flexible robots based on deep learning," *IEEE Trans. Robot.*, vol. 39, no. 2, pp. 1580–1593, Apr. 2023.

[20] B. K. Horn, "Closed-form solution of absolute orientation using unit quaternions," *Josa A*, vol. 4, no. 4, pp. 629–642, 1987.

[21] J. A. Roulier, "Specifying the arc length of Bézier curves," *Comput. Aided Geometric Des.*, vol. 10, no. 1, pp. 25–56, 1993.

[22] T. M. Le, B. Fatahi, H. Khabbaz, and W. Sun, "Numerical optimization applying trust-region reflective least squares algorithm with constraints to optimize the non-linear creep parameters of soft soil," *Appl. Math. Modelling*, vol. 41, pp. 236–256, 2017.

[23] J. J. Moré, "The Levenberg-Marquardt algorithm: Implementation and theory," in *Proc. Numer. Anal.*, 1978, pp. 105–116.

[24] J. Cao, K. A. Novstrup, A. Goyal, S. P. Midkiff, and J. M. Caruthers, "A parallel Levenberg-Marquardt algorithm," in *Proc. 23rd Int. Conf. Supercomputing*, 2009, pp. 450–459.

[25] Q. M. De Ruiter, C. M. Gijsberts, C. E. Hazenberg, F. L. Moll, and J. A. V. Herwaarden, "Radiation awareness for endovascular abdominal aortic aneurysm repair in the hybrid operating room. an instant patient risk chart for daily practice," *J. Endovascular Ther.*, vol. 24, no. 3, pp. 425–434, 2017.

[26] D. Chetverikov, D. Svirko, D. Stepanov, and P. Krsek, "The trimmed iterative closest point algorithm," in *Proc. IEEE Int. Conf. Pattern Recognit.*, 2002, pp. 545–548.